

Influence of the viscosity of poly(methyl methacrylate) on the cellular structure of nanocellular materials

Judith Martín-de León,^{a*} Victoria Bernardo,^a Ester Laguna-Gutiérrez^b and Miguel Ángel Rodríguez-Pérez^{a,c}



Abstract

Three different grades of poly(methyl methacrylate) (PMMA) with different rheological properties are used for the production of nanocellular materials using gas dissolution foaming. The influences of both the viscosity of the different polymers and the processing parameters on the final cellular structure are studied using a wide range of saturation and foaming conditions. Foaming conditions affect similarly all cellular materials. It is found that an increase of the foaming temperature results in less dense nanocellular materials, with higher cell nucleation densities. In addition, it is demonstrated that a lower viscosity leads to cellular polymers with a lower relative density but larger cell sizes and smaller cell nucleation densities, these differences being more noticeable for the conditions in which low solubilities are reached. It is possible to produce nanocellular materials with relative densities of 0.24 combined with cell sizes of 75 nm and cell nucleation densities of 10^{15} nuclei cm^{-3} using the PMMA with the lowest viscosity. In contrast, minimum cell sizes of around 14 nm and maximum cell nucleation densities of 3.5×10^{16} nuclei cm^{-3} with relative densities of 0.4 are obtained with the most viscous one.

© 2019 Society of Chemical Industry

Supporting information may be found in the online version of this article.

Keywords: nanocellular PMMA; viscosity; rheology; gas dissolution foaming

INTRODUCTION

Nowadays, the continuing evolution of technology requires the production of materials with tailor-made properties. Cellular polymers are very prominent in this evolution due to an uncommon combination of properties combined with their low weight, and therefore the possibility of reducing costs. Particularly, microcellular polymers have gained increasing importance since their discovery in the early 1980s,¹ because of their enhanced mechanical properties in comparison with conventional cellular polymers, their higher thermal stability and their reduced thermal conductivity.^{2,3} These improvements have encouraged scientists in the field of cellular materials to further reduce the cell size to obtain better materials. Thus, nanocellular polymers were born, bringing with them a new enhancement of mechanical properties such as a further reduction of the thermal conductivity as well as new and promising properties such as the possibility of producing transparent cellular polymers.^{4–6}

Even though nanocellular polymers are, in general, better than microcellular polymers, their interesting properties also depend on the cell size and the density among other characteristics (such as open-cell content or anisotropy). For instance, the Knudsen effect starts to be significant for cell sizes smaller than 100 nm. Besides, the thermal conductivity of nanocellular polymers starts to be competitive with that of the ones currently on the market for relative densities smaller than 0.15.^{4,7} On the other hand, when referring to the transparency of these cellular materials, more demanding requirements are needed, cell sizes smaller than 50 nm

are needed, and it also expected that this property would strongly depend on the cellular material density.⁸

Therefore, it is mandatory to acquire a fine control of the process of the design of nanocellular polymers with the right density and cell size, and, in this sense, it is also needed to find simple approaches to obtain that control. In particular, it has been proven that the viscosity of the polymer matrix is crucial for all the steps in the production of cellular and microcellular materials; that is, nucleation, growth, degeneration mechanisms of the cellular structure and stabilization are affected by this property of the solid material.^{9–11} The viscosity of the base material can be easily modified during the polymerization process or by using fillers or chain extenders, among other methods. Taking into account the previous results for cellular polymers and microcellular polymers, there could be a simple way to obtain nanocellular materials with different cellular structures for given production conditions.^{12,13}

* Correspondence to: JM-de León, Condensed Matter Physics Department, Science Faculty, University of Valladolid. Paseo de Belén 7, 47011, Valladolid, Spain. E-mail: jmadeleon@fmc.uva.es

a Condensed Matter Physics Department, Cellular Material Laboratory (CellMat), Universidad de Valladolid, Valladolid, Spain

b CellMat Technologies SL, Valladolid, Spain

c Instituto BIOECOUMA, Universidad de Valladolid, Valladolid, Spain

The study of the production of nanocellular materials has been carried out using various polymer matrices such as polycarbonate,¹⁴ polyphenylsulfone,¹⁵ polyetherimide¹⁵ or, one of the most promising, poly(methyl methacrylate) (PMMA).¹⁶ With this last one, multiple strategies have been followed, trying to optimize the final cellular structure. One strategy has been the use of various copolymers based on PMMA, for example, PMMA/MAM blends (PMMA with block copolymer PMMA-*co*-poly(butyl acrylate)-*co*-PMMA (MAM))^{17,18} or P(MMA-*co*-EMA) (a random copolymer of MMA with 50 wt% ethyl methacrylate).¹⁹ Another strategy has been the use of nanocomposites with nanometric particles such as sepiolites²⁰ or silica particles.²¹ Finally, the modification of the processing parameters has also been studied to achieve an optimum cellular structure and density.^{16,22,23}

However, studies regarding the influence of the viscosity of the base material on the final cellular structure are hard to find in the literature. As far as the authors know, there exist only two previous reports. In the first one, Forest *et al.* discussed this topic.¹³ PMMA/MAM blends were used in that work. Despite the nanocellular structure being governed by the presence of MAM phase due to a heterogeneous nucleation process, it was demonstrated that the viscosity of the PMMA phase used affected the final cellular structure, a low PMMA viscosity being favourable for reaching low densities, but not so low as to prevent coalescence leading to the loss of the nanocellular structure.

Costeux *et al.*¹² presented the cellular structure of several blends of polymers with various viscosities. A lower viscosity, it is also claimed, leads to a smaller relative density. However, results were not directly correlated with the viscosity of the final blend.

An essential difference of the present work from that of Forest *et al.*,¹³ apart from the much broader processing conditions used in our case, is that for the systems analysed here homogeneous nucleation takes place, and this type of nucleation could also depend on the properties of the base polymer. Referring to the work of Costeux *et al.*, one-step foaming was used in the process; moreover, polymer blends instead of single polymers were used. This leads to there being no possibility of relating the obtained results to the viscosity of the system due to the behaviour of this viscosity under gas pressure being different for each polymer. In the work reported here, all those contributions were removed by using different polymers in a two-step gas dissolution foaming process.

Bearing the previous considerations in mind, the main target of the work reported here was to study the influence of both the viscosity of homogeneous PMMA grades and the processing parameters on the final cellular structure. A complete relationship between the properties of the polymer matrix, the processing parameters and the final cellular structure has been established. It has also been found that the viscosity of the starting polymer can be used to fine-tune the cellular structure of the resulting nanocellular polymer.

MATERIALS AND METHODS

Materials

Three different grades of PMMA were used for this study: V825T, 7N and 6N. V825T was kindly supplied by ALTUGLAS® International (Colombes, France) in the form of pellets, while 7N and 6N were kindly provided by PLEXIGLAS® Evonik Industries (Essen, Germany). All the materials used had a density (ρ) of 1.19 g cm⁻³ (measured at 23 °C and 50% relative humidity). They are named as HV (high viscosity), MV (medium viscosity) and LV (low

viscosity). Medical-grade CO₂ (99.9% purity) was used as a blowing agent.

Sample production

Pellets were used to produce compression-moulded sheets of 2 mm in thickness using a hot plate press from Remtex (Barcelona, Spain). Before this process, PMMA was dried at 80 °C for 4 h to eliminate any moisture in the polymer. The compression-moulding process comprised three steps. Firstly, PMMA was heated at 250 °C for 9 min without applying any pressure. Secondly, the material was subjected to constant pressure of 11 MPa for 1 min. Finally, the 2 mm thick layer was cooled at room temperature and at a pressure of 11 MPa.

The obtained cylindrical sheets were cut into 20 × 20 × 2 mm³ samples to proceed with the foaming experiments.

The same procedure was used for the production of samples of 1 mm in thickness for rheological measurements.

Foaming tests

Different cellular materials were produced using a gas dissolution foaming process. This process consisted of three steps. Firstly, in the saturation step, the samples were saturated, for a long enough time (t_{sat}) to reach the solubility limit in the whole volume of the sample, under a certain saturation pressure (P_{sat}) and saturation temperature (T_{sat}) of CO₂. Secondly, the pressure was released, and the samples were transferred to the last step, the foaming step. The time between the pressure release and foaming is called the desorption time (t_d). During the third step, samples were immersed in a thermal bath at the foaming temperature (T_f) for the foaming time (t_f) to promote the foaming process.

In this work, two different set-ups were used, one for saturation experiments at room temperature and the other for performing experiments using saturation temperatures below room temperature. For the room temperature experiments, a pressure vessel (PARR 4681) provided by Parr Instrument Company (Moline, IL, USA) was used. Moreover, to provide the desired pressure, the system comprised a pump (SFT-10) supplied by Supercritical Fluid Technologies Inc. (Newark, DE, USA).

For the experiments carried out at low temperature, a PARR 4760 pressure vessel was employed. This autoclave was also provided by Parr Instrument Company (Moline, IL, USA) and it was placed inside a freezer that allows reaching temperatures from -15 to -32 °C.

For all saturation experiments, samples were foamed in a thermal bath (J. P. Selecta model 600685, Grupo Selecta, Barcelona, Spain).

As shown in Fig. 1, different saturation parameters, as well as different foaming conditions, were used in this work. For saturation parameters, four different conditions were used. The experiments with 31 MPa and 24 °C saturation conditions were performed in the room temperature set-up by saturating for 24 h. In this particular system, the pressure drop rate was 100 MPa s⁻¹. On the other hand, the experiments at -32 °C and saturation pressures of 6, 10 and 20 MPa were carried out in the set-up for low-temperature saturation. Saturation time was 15 days, and the pressure drop rates were 10, 31 and 75 MPa s⁻¹.

Moreover, for each of these saturation parameters, four different foaming conditions were used. Samples were foamed during 1 min at temperatures of 25, 40, 60 and 80 °C. Desorption time was 2 and 1 min, respectively, for the room temperature and low-temperature set-ups. In short, 16 different conditions were used for each material to study their influence on the final cellular structure.

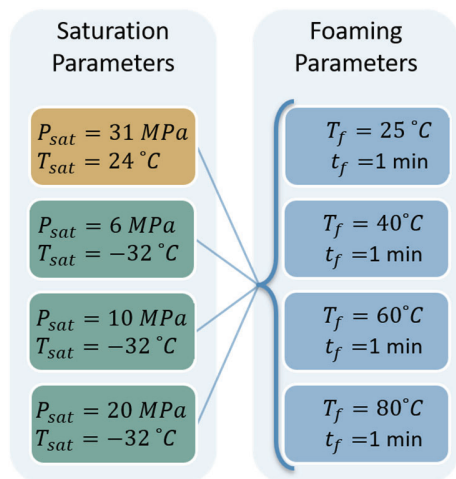


Figure 1. Production conditions for the cellular materials produced in this work.

Characterization techniques

Glass transition temperature

The glass transition temperature (T_g) was determined using a Mettler DSC30 differential scanning calorimeter previously calibrated with indium. The value of this temperature was considered as the mid-point of the drop in the thermogram that characterizes this transition. The selected weight for all the samples was 5 mg. Samples were heated from 20 to 160 °C at 10 °C min⁻¹.

Solubility and diffusivity

Solubility is defined as the amount of gas uptake and was determined as the percentage weight increase of each sample due to gas sorption. The desorption curve (mass lost *versus* time) was recorded using a Mettler-Toledo balance and was used to extrapolate to zero time the mass of the samples after saturation. This value is considered as the mass of the sample when it is fully saturated, from which the solubility of the material is calculated.²⁴

Moreover, the desorption curve was used to determine the desorption diffusivity using the slope method.²⁵

Density

The density of the solid samples (ρ_s) was determined using a gas pycnometer (AccuPyc II 1340, Micromeritics, Norcross, GA, USA). The density of the foamed samples was measured with a density determination kit for an AT261 Mettler-Toledo balance considering the water displacement method based on the Archimedes principle. Solid skins of the nanocellular polymers were removed before these measurements by polishing more than 200 μ m on each side of the samples.

Relative density (ρ_r) was defined as the ratio between ρ_f and ρ_s ($\rho_r = \rho_f/\rho_s$).

Open-cell content

To measure the percentage of open cells in the cellular materials, namely the open-cell content (O_v), a gas pycnometer (AccuPyc II 1340, Micromeritics) was used following the procedure described in ASTM D6226-10 standard. The value of this parameter is given by

$$O_v = \frac{V - V_p - V_s}{V(1 - \rho_r)} \quad (1)$$

where V is the geometric volume of the sample (determined by means of $V = m/\rho$ with an AT261 Mettler-Toledo balance), V_p is the volume determined by the pycnometer and V_s considers the exposed cells at the surface of the sample, a value that is negligible for nanocellular materials. To determine V_p , a pressure scan from 0.2 to 1.3 MPa was performed measuring the volume for each pressure. This leads to a set of volumes as a function of pressure. Up to a certain point the volume becomes constant, meaning that no more gas can penetrate inside the cells of the cellular material. V_p is calculated as the average value of those latter constant measured volumes.

Scanning electron microscopy

The cellular structure of the samples was visualized with an environmental SEM instrument (QUANTA 200 FEG, Hillsboro, OR, USA). The samples were prepared for visualization following different steps. Firstly, they were fractured after immersion in liquid nitrogen. Then, they were coated with 5 nm of gold using a sputter coater (SDC 005, Balzers Union, Balzers, Liechtenstein). Finally, they were observed using the environmental SEM instrument.

The cellular structure was analysed with software based on ImageJ/FIJI²⁶ affording the cell size (ϕ), the standard deviation of the cell size distribution (SD) and the cell nucleation density (N_0) (calculated using Kumar's method²⁷) of each cellular material. SEM images were obtained along the thickness of each sample to ensure homogeneity. At least three different images and more than 200 cells per cellular material were analysed. For each measured image values for N_0 and ϕ were obtained. Finally, the data presented in the paper for each material correspond to the mean value of three images. The standard deviation of the three measurements was calculated and added in the form of an error bar.

Polymer rheology

Zero-shear viscosity η_0 was determined using shear rheology. The measurements were carried out with a stress-controlled rheometer (AR 2000 EX, TA Instruments). Solid cylindrical samples were prepared by compression molding using the procedure explained above. Dynamic shear viscosity measurements were performed at 230 °C under a nitrogen atmosphere and using a parallel-plate geometry of $R = 25$ mm in diameter and a fixed gap of $h = 1$ mm. The angular frequency range was $0.01 < \omega < 100$ rad s⁻¹, and a strain of 6% was used. From the dynamic shear viscosity measurements, the zero-shear viscosity was calculated as the value of the complex viscosity at low frequencies in the Newtonian plateau.²⁸

RESULTS

Properties of solid matrix

To determine the differences between the three solid PMMA samples under study, the molecular weight as well as the polydispersity index ($r = M_w/M_n$), determined using gel permeation chromatography measurements, were analysed. Moreover, the glass transition temperature, the melt flow index (measured at 160 °C and 10 kg) and the zero-shear viscosity were evaluated.

As evident from Table 1, differences in the molecular weight are not so noticeable between the three polymers. However, when analysing the polydispersity index, it can be seen that although the molecular weight of HV is smaller than that of MV, the molecular weight distribution is wider for HV.

Table 1. Molecular weight, polydispersity index, melt flow index and zero-shear viscosity for the three grades of PMMA

Material	M_w (g mol ⁻¹)	M_n (g mol ⁻¹)	$r = M_w/M_n$	T_g (°C)	MFI (g (10 min) ⁻¹)	η_0 (Pa s)
HV	83 221	43 157	1.93	114.4	1.92	7095
MV	83 621	45 119	1.85	109.3	3.64	3800
LV	77 255	39 149	1.97	98.6	8.20	1587

On the other hand, the three different grades of PMMA show clear differences when referring to the glass transition temperature, the melt flow index and the zero-shear viscosity. PMMA sample HV presents higher values, with T_g of 114.4 °C and a zero-shear viscosity of 7095 Pa s. MV and LV have smaller values with T_g of 109 and 99 °C, respectively, and a zero-shear viscosity of 3800 and 1587 Pa s. Hence, there is a 15 °C difference between T_g of the HV and LV materials. Besides, the ratio of viscosities at 230 °C is significant; the HV grade has 2.4 times higher viscosity than the MV grade and a value 4.5 times higher than that of the LV grade.

These differences in the physical properties of the raw materials will be essential for understanding the different behaviour of each material in the foaming process.

Solubility and diffusivity

As was proven in previous works,¹⁶ the solubility and diffusivity of CO₂ changes with the saturation conditions used. In order to study this change with the saturation conditions used and to establish the differences between materials, the magnitudes of both parameters were determined as explained in the Materials and Methods section.

Figure 2(a) shows the solubility of the materials under study for the four saturation conditions used. As expected, the results show that a change in the saturation temperature from 24 to -32 °C leads to a significant increase in the solubility for the three polymers. On the other hand, when fixing the saturation temperature at -32 °C, an increase in the saturation pressure also results in a solubility increase. The highest values reached are around 45% for 20 MPa and -32 °C.

If the differences among materials are analysed, it can be said that for the experiments carried out at low saturation temperatures the three materials show very similar values of solubility; however, for the experiment at 24 °C, the material with the lowest viscosity shows a higher solubility (36 wt% versus 31 wt%).

Taking into account Eqn (2), the increase in solubility when saturation temperature is reduced from 24 to -32 °C is expected:

$$S = S_0 \exp\left(-\frac{\Delta H_s}{RT}\right) \quad (2)$$

Also, when maintaining the saturation temperature at -32 °C, an increase in the saturation pressure increases the amount of gas uptake, which is in agreement with previous results for similar systems.^{17,29,30}

Differences between materials can be explained by considering the physical mechanisms taking place during gas sorption. Solubility depends on the polar interaction between the gas and the polymer and on the free volume available in the PMMA. The relative weight of these two contributions depends on the saturation temperature. At low saturation temperatures, the polar interactions between the gas and the polymer are more important, while at high saturation temperatures the influence of the polar interactions decreases and the free volume of the polymer has a more substantial influence on the solubility.³¹

The free volume (proportional to $T_{sat} - T_g$ ³²) of LV is higher than that of MV and HV (Table 1). Thus at a saturation temperature of 24 °C, this polymer presents a higher solubility, while at -32 °C the solubility of all the grades is equal due to free volume losing importance.

The desorption diffusivity (Fig. 2(b) increases with solubility, the values being similar for the three materials under study. A higher solubility results in a higher CO₂ concentration gradient between the sample and the atmosphere, leading to fast desorption.³³

Relative density and cellular structure

Figure 3 shows representative SEM images of the samples produced using the three raw materials (see Fig. S1 in the supporting information for additional images). It can be seen that all the produced cellular materials show a homogeneous nanocellular structure. Additionally, it can be observed that samples produced from LV at 31 MPa and 24 °C present a wider cell size distribution than those produced from HV and MV. When calculating SD/ϕ parameter, this material shows values near 0.5, while HV and MV present values around 0.3. This difference disappears when saturating at temperatures below zero.

Although the nanocellular structure is homogeneous for the three materials, there are apparent differences when changing the process parameters or the characteristics of the PMMA. This section is focused on an in-depth study of the influence of both the processing parameters and the viscosity of the PMMA on the final cellular structure.

Influence of processing parameters

Influence of solubility. As is evident from Fig. 3, considerable differences in the cellular structure of the PMMA samples are found when the saturation conditions and, consequently, the solubility are modified. To illustrate this fact, the cell nucleation density, the cell size, the relative density and the open-cell content were studied as a function of the solubility for all foaming conditions. To show these results, a foaming temperature of 60 °C has been selected (Fig. 4), the tendency being very similar for the other foaming temperatures (supporting information, Figs S2–S5).

For the three grades of PMMA, cell nucleation density increases with solubility while the value of the cell size decreases. The most significant change is observed in the first increase of solubility (from 33 to 39 wt% of CO₂ uptake for LV and from 36 to 39 wt% for MV and HV). Although the saturation pressure, between these two levels, decreases from 31 to 6 MPa, the decrease of the saturation temperature from 24 to -32 °C results in an increase of almost two orders of magnitude in the cell nucleation density of all the cellular materials while the cell size decreases by around five times. As can be seen, the cell size reduces from hundreds of nanometres to tens of nanometres.

A further increase in the solubility caused by an increase in the saturation pressure from 6 to 20 MPa (when the saturation

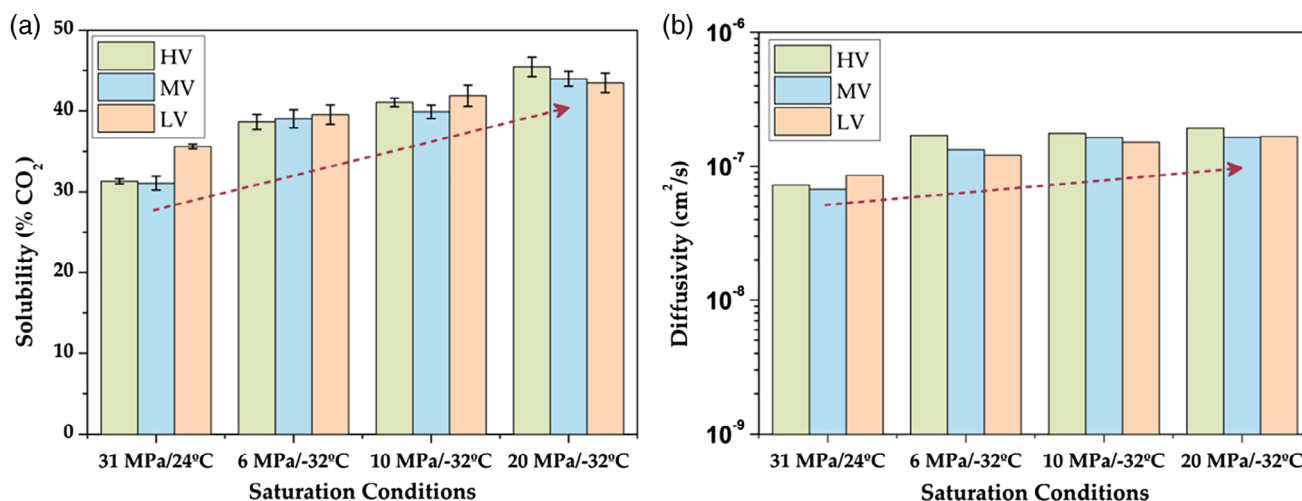


Figure 2. (a) Solubility of the three PMMA grades as a function of the saturation conditions. (b) Desorption diffusivity of the three PMMA grades as a function of the saturation conditions. Arrows indicate the increase in the magnitudes of both.

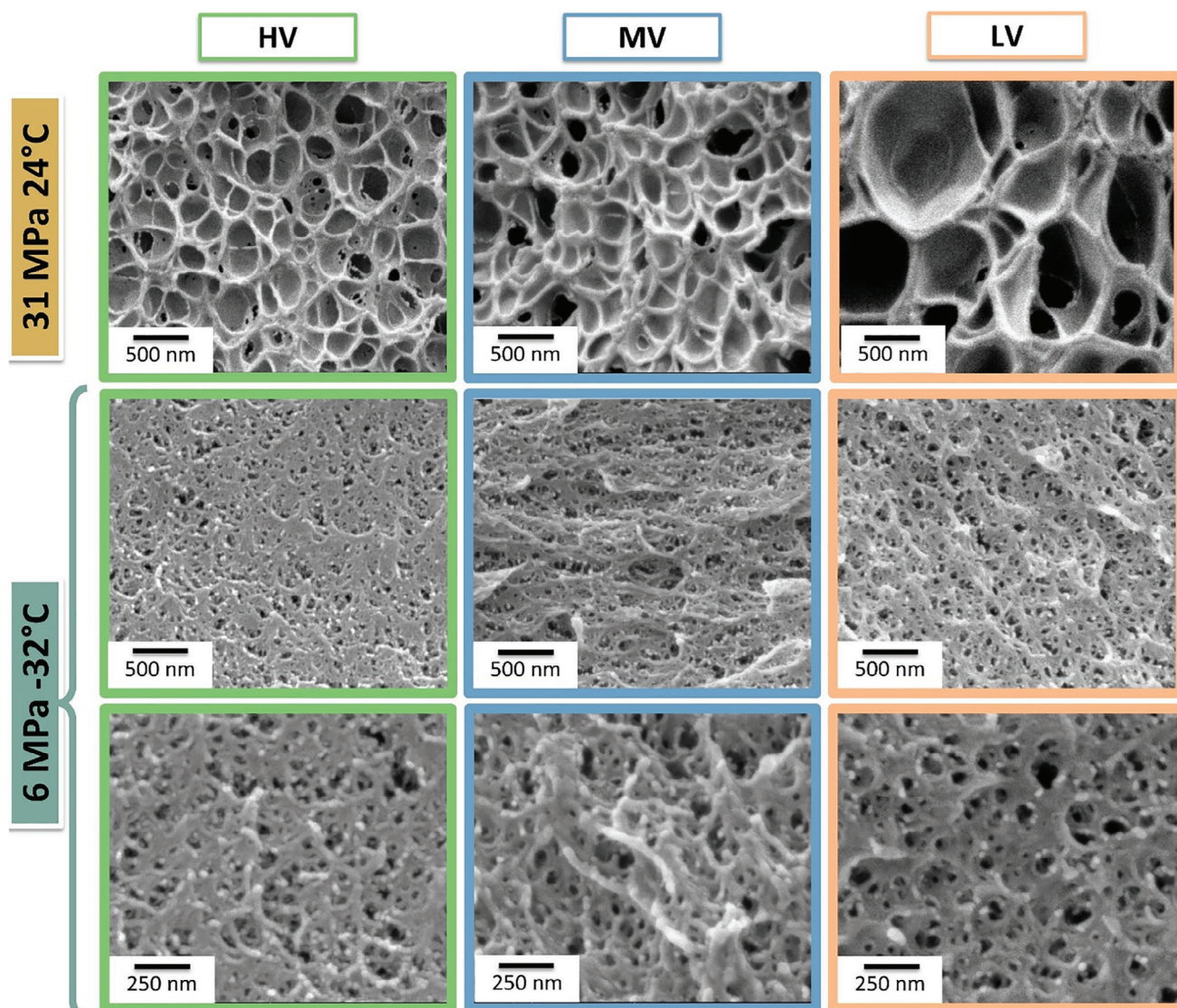


Figure 3. SEM micrographs for the three materials for two saturation conditions (30 MPa, 25 °C and 6 MPa, -32 °C) foamed at 60 °C during 1 min.

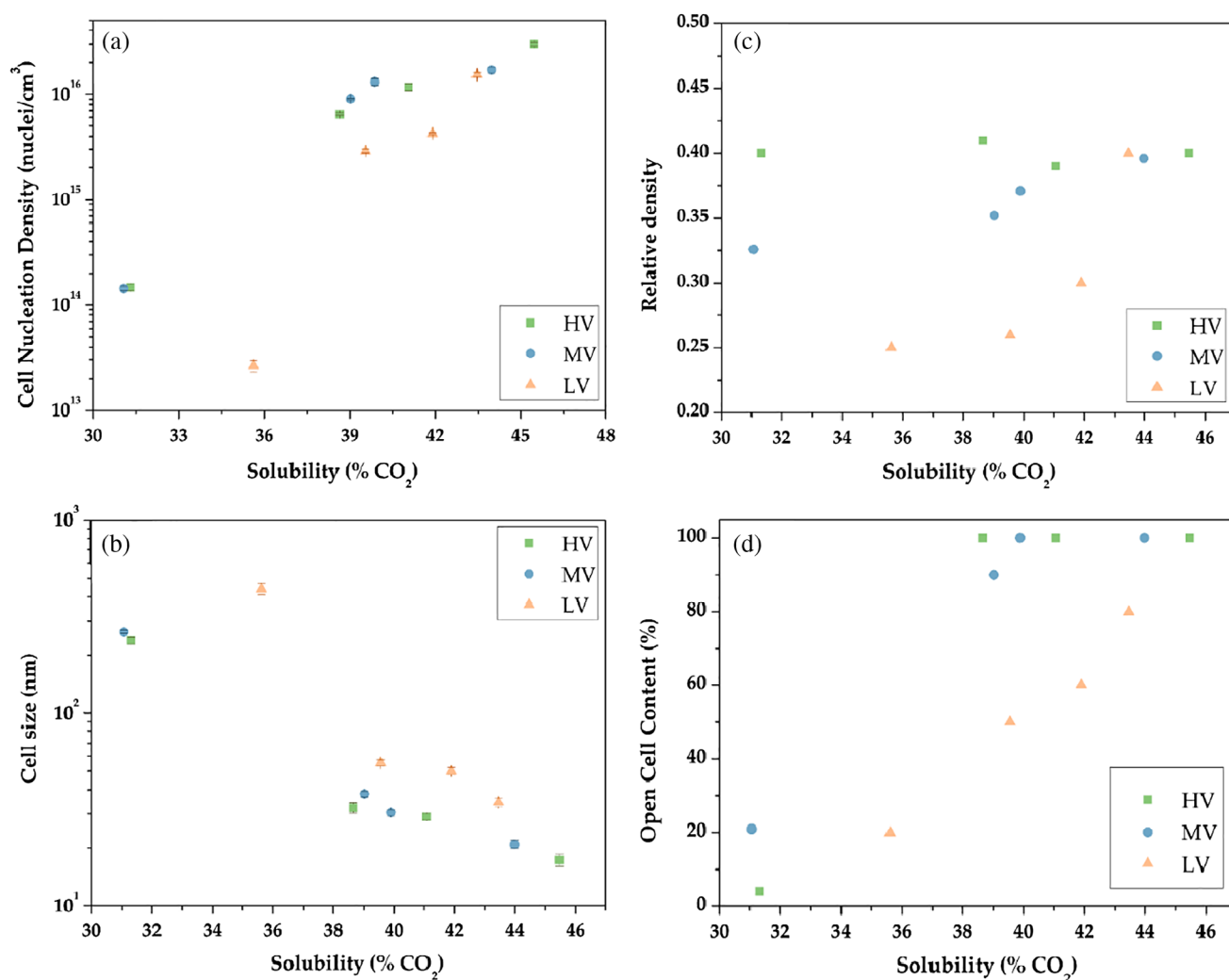


Figure 4. (a) Cell nucleation density, (b) cell size, (c) relative density and (d) open-cell content as a function of solubility.

temperature is fixed at $-32\text{ }^{\circ}\text{C}$) produces an additional increase in the cell nucleation density for the three PMMA grades. Thus, when the saturation pressure is 20 MPa, the cell nucleation density increases up to values higher than 10^{16} nuclei cm^{-3} for the three materials while cell size is reduced to values of around 15 nm for HV, 20 nm for MV and 30 nm for LV.

These changes in the cellular structure affect the relative density (Fig. 4(c)). However, the trends are, in this case, different depending on the PMMA under study. For HV, the relative density remains almost constant at around 0.4 independent of the saturation conditions. However, for LV and MV materials, the relative density increases when the solubility becomes higher, meaning that, as the solubility increases, the ability to expand seems to be reduced for these two materials.

These results can be understood considering that increasing the number of nucleation points implies a reduction in the relative density, but a reduction of the cell size leads to an increase in the relative density. Thus, both contributions compete in the evolution of ρ_r . For HV the relative density remains constant due to an equilibrium between increasing N_0 and decreasing ϕ ; for MV and LV the reduction of cell size is more significant than the increase of cell nucleation density leading to a density increase as solubility increases.

Considering Fig. 4(d), the different ability of the cellular materials to expand is closely linked with the open-cell content of the cellular materials produced. A lower solubility leads to cellular materials with a small open-cell content, while higher solubility leads to completely interconnected cellular structures for HV and MV, and medium to high open-cell contents for LV. It has been previously reported²² that the interconnectivity of the cellular structure promotes faster desorption of gas, preventing further expansion. So those cellular materials with an intermediate or a closed-cell cellular structure have a high ability to expand and therefore present lower relative densities. In short, an increase of solubility leads to nanocellular materials with a greater number of interconnected and smaller cells, and therefore with a higher relative density. A more in-depth discussion of the influence of the type of material is presented below in the section on the influence of the rheological properties of PMMA.

Influence of foaming parameters. As discussed above, T_g is different for the three materials under study. For this reason, in order to study the influence of the foaming temperature on the final cellular structure, the relative densities for all the saturation conditions have been determined as a function of the difference between T_g and the foaming temperature ($T_g - T_f$). As can be seen in Fig. 5, the

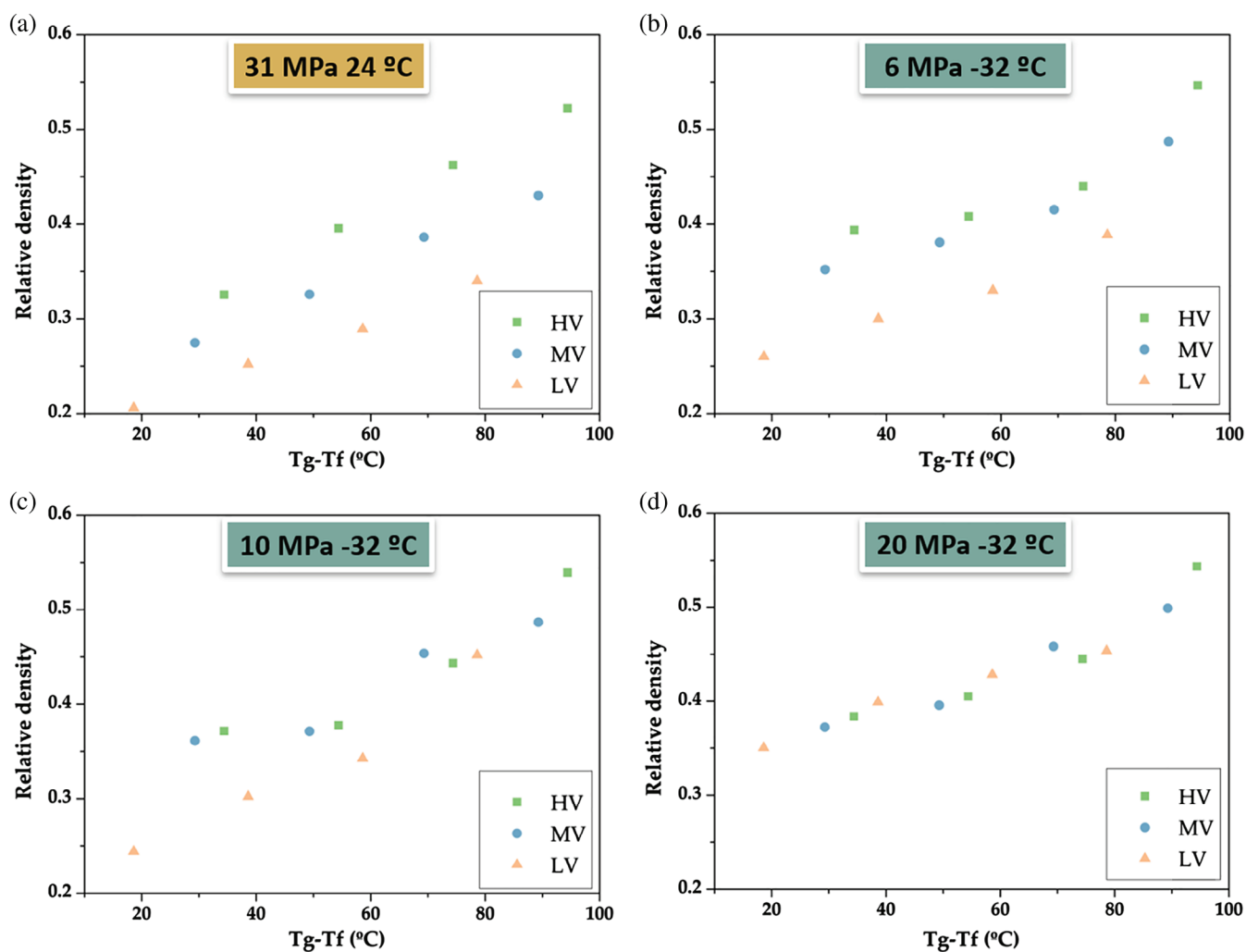


Figure 5. Relative density as a function of the difference between glass transition temperature and foaming temperature for all saturation conditions.

relative density strongly depends on this temperature difference. An increase in T_f results in a decrease of the relative density for all the cellular materials produced.²²

Changes between saturation conditions are also observed in Fig. 5. The diffusion of gas inside the polymer implies a reduction of T_g , up to the so-called effective glass transition temperature $T_{g,eff}$. This reduction is the result of an increase in the polymer chain mobility when the gas occupies the free volume of the polymer. LV presents higher solubilities except for saturation conditions of 20 MPa and $-32\text{ }^\circ\text{C}$, which presumably leads to the smallest $T_{g,eff}$ that could be the reason for the smaller relative density in comparison with the values for HV and MV observed in Figs 5(a)–(c).

An increase of the foaming temperature up to $100\text{ }^\circ\text{C}$ leads to the degeneration of the cellular structure for all the materials and saturation conditions except in the case of 31 MPa and $24\text{ }^\circ\text{C}$. For this latter condition, degeneration occurs at $110\text{ }^\circ\text{C}$.²²

To understand the reasons for this clear modification in the relative density, the cellular structure of all the nanocellular materials has been characterized. Figure 6 shows both the cell nucleation density and cell size as a function of relative density for two different saturation conditions: 31 MPa and $24\text{ }^\circ\text{C}$ and 20 MPa and $-32\text{ }^\circ\text{C}$. The reduction in relative density (Fig. 5) is connected to an increase in the number of nucleation points while the cell size maintains almost constant.

When talking about the cellular materials saturated at 31 MPa and $24\text{ }^\circ\text{C}$, HV goes from cell sizes of 200 nm and cell nucleation densities of 1.5×10^{14} nuclei cm^{-3} for a relative density of 0.5 to cell sizes of 225 nm and cell nucleation densities of 3.5×10^{14} nuclei cm^{-3} , which means that N_0 is doubled while cell size slightly increases. Similarly, LV changes from 1.8×10^{13} nuclei cm^{-3} when the relative density is 0.34 to 3.3×10^{13} nuclei cm^{-3} when it decreases to 0.21, while cell sizes are between 450 and 490 nm for all densities. The same can be said when saturating at 20 MPa and $-32\text{ }^\circ\text{C}$, where cell nucleation densities are doubled between the density extremes while cell size is maintained at around 17 nm for HV, 20 nm for MV and 35 nm for LV. Similar results were also observed for the saturation conditions of 6 MPa, $-32\text{ }^\circ\text{C}$ and 10 MPa, $-32\text{ }^\circ\text{C}$ (supporting information, Fig. S6).

Summing up, the reduction of the relative density is mainly caused by an increase of the cell nucleation density triggered by an increase of the foaming temperature. This is a common trend for all the PMMA samples under study. In particular, a change in the foaming temperature from 25 to $80\text{ }^\circ\text{C}$ allows an increase in the cell nucleation density by two times while cell size remains almost constant. In this way, for the more extreme saturation conditions, 20 MPa and $-32\text{ }^\circ\text{C}$, it is possible to achieve values of N_0 as high as 10^{16} nuclei cm^{-3} and cell sizes smaller than 40 nm for all the materials under study.

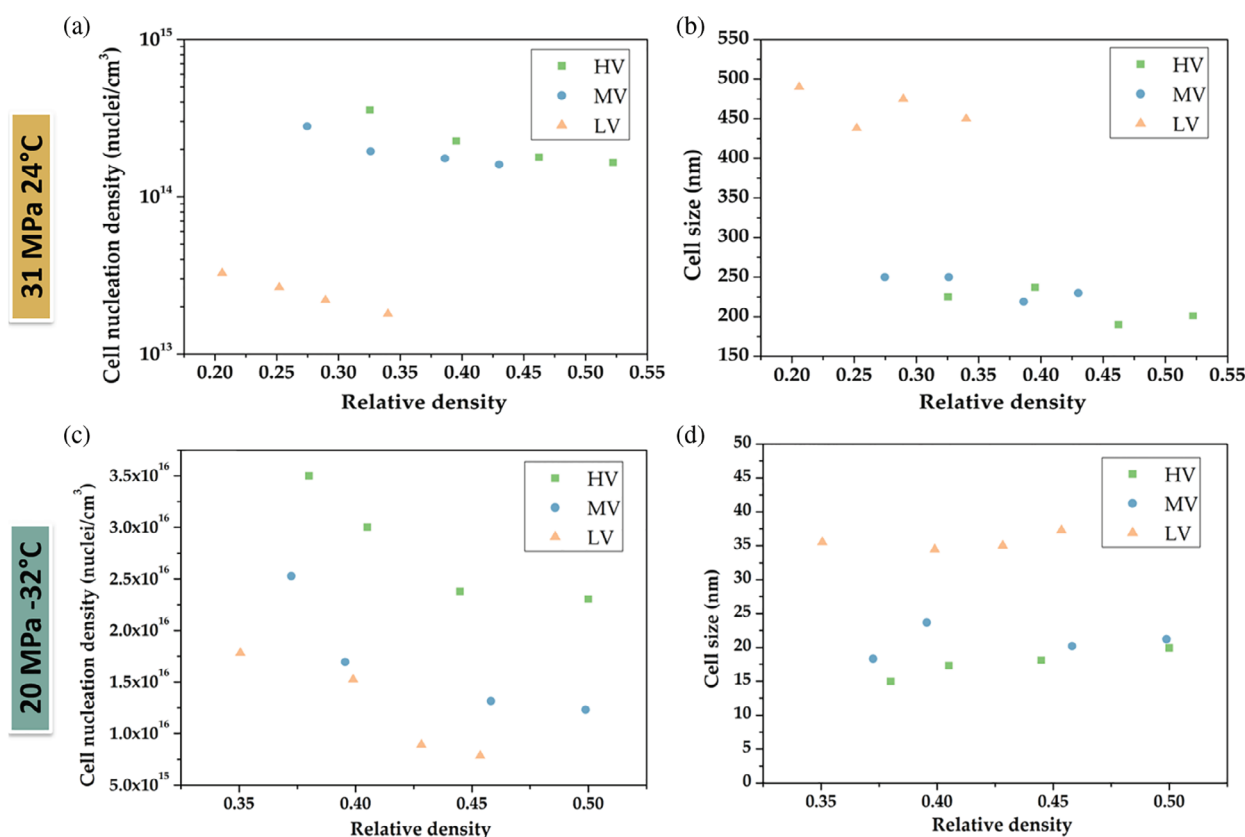


Figure 6. (a) Cell nucleation density and (b) cell size as a function of relative density for 31 MPa and 24 °C saturation conditions. (c) Cell nucleation density and (d) cell size as a function of relative density for 20 MPa and -32 °C saturation conditions.

In short, it can be said that the foaming temperature has a substantial effect on the nanocellular materials produced using PMMA as polymer matrix. An increase of the foaming temperature results in an increase in the cell nucleation density while the cell size is maintained; this is reflected in a reduction of the density of the final cellular material (Fig. 5).

Influence of rheological properties of PMMA

From the previous section, it is evident that, although the trends for the process parameters are very similar for all the analysed cellular materials, there are clear differences in the absolute values of the foam characteristics depending on the type of PMMA. This section is focused on a study of the modifications of the final cellular structure as a function of the zero-shear viscosity of the raw polymers.

Figure 7 shows those differences: the relative density, the cell nucleation density and the cell size of all the cellular materials produced (for all the conditions in Fig. 1) are plotted as a function of the zero-shear viscosity. It seems clear that the zero-shear viscosity is establishing some boundaries that are different for each material and foam characteristic.

The material that allows the reaching of a smaller density is the LV one, while the ability to expand is harder with an increase of the viscosity of the raw PMMA matrix. Thus, for LV, a density as low as 0.21 has been reached, while for HV the minimum density produced in this work is been 0.33.

On the other hand, a smaller zero-shear viscosity makes it possible to have available a broader range of cell nucleation densities and cell sizes. Then, it is possible to have cellular materials with

cell sizes from 491 to 35 nm and N_0 from 2.2×10^{13} to 1.8×10^{16} nuclei cm^{-3} when working with LV; these ranges are reduced to 225 to 14 nm and 1.5×10^{14} to 3×10^{16} nuclei cm^{-3} for HV. Nonetheless, a higher viscosity allows the reaching of higher cell nucleation densities and lower cell sizes.

It is also vital to notice that differences between materials are more pronounced at low solubilities (Fig. 6) causing the lower limit in the cell nucleation density (corresponding to the saturation conditions of 31 MPa and 24 °C) to be more variable among the three materials. In addition, the upper limit in the cell size (also for 31 MPa and 24 °C) presents more differences between cellular materials than the lower one (20 MPa and -32 °C). In conclusion, at high solubilities, the three materials behave more similarly in terms of cellular structure characteristics.

In order to understand the results discussed above, it is necessary to consider the nucleation mechanisms. It has been already proven that the classical nucleation theory (CNT), although providing correct trends, is useless for predicting absolute data for nanocellular polymers. Moreover, viscoelastic effects are not considered in CNT. Costeux *et al.*³⁴ proposed a model based on CNT. This new model introduces some necessary changes for the understanding of nanocellular foaming.

This theory introduces a new concept, the influence volume (IV). This new idea states that when a stable nucleus is formed, the surrounding gas molecules start to diffuse into this nucleus. This diffusion leads to a gas concentration gradient from the nucleus surface, as shown in Fig. 8(a). Thus, near the surface of the nascent cell, the concentration of gas is smaller, increasing as one moves away from the surface to reach a value C_0 corresponding to the

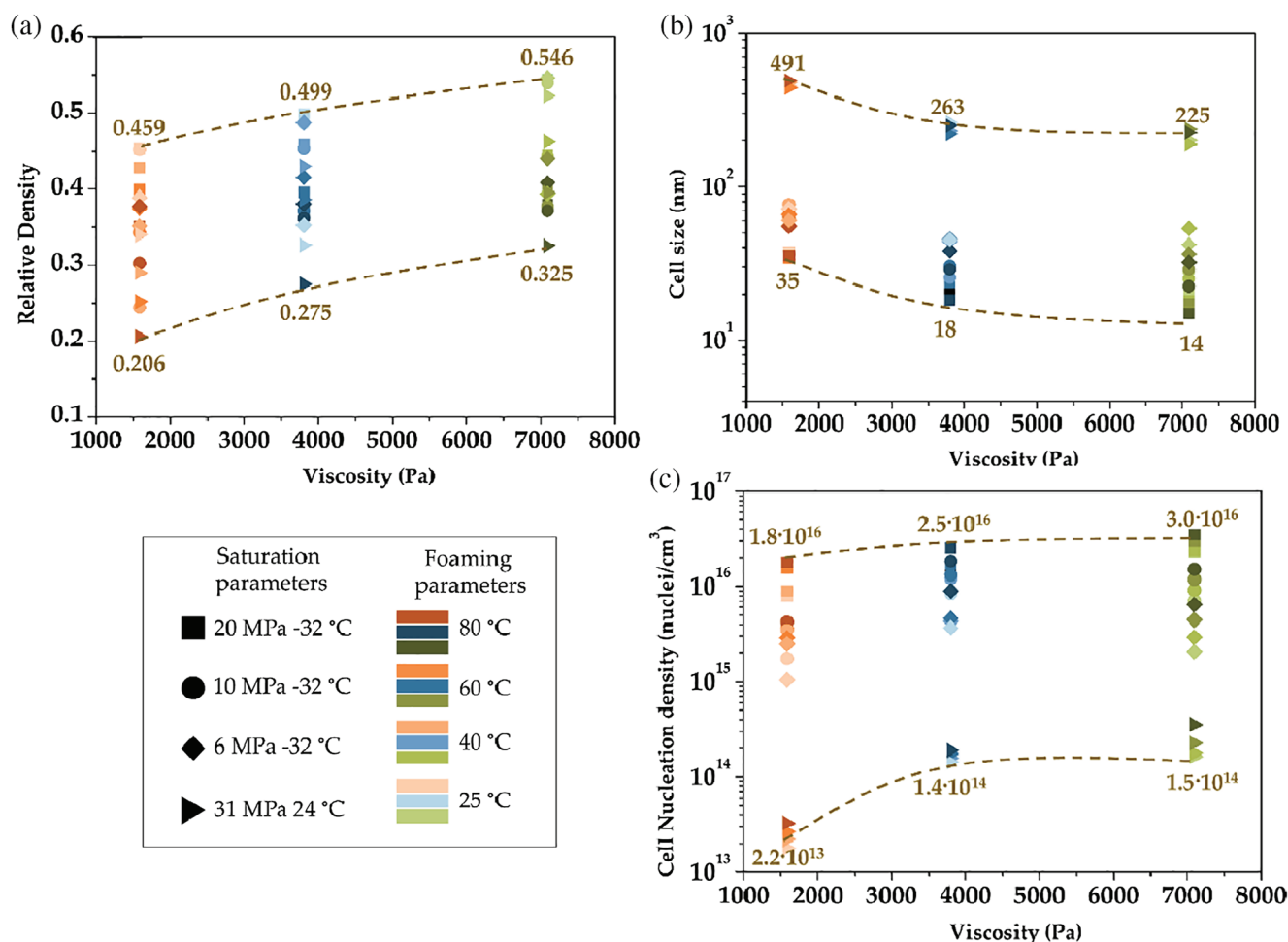


Figure 7. (a) Relative density, (b) cell size and (c) cell nucleation density as a function of zero-shear viscosity. The data for all the experiments performed have been included in these plots. For a given viscosity and polymer, the different data were obtained by modifying the saturation conditions and the foaming temperature.

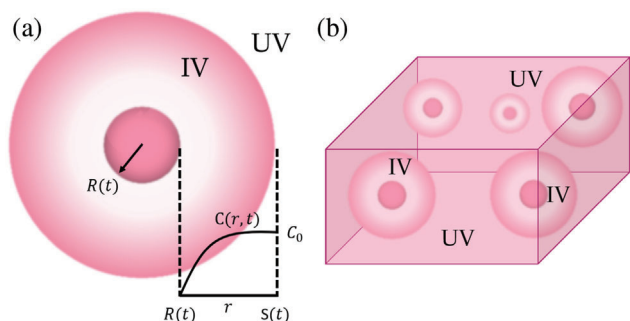


Figure 8. The concept of IV in the nucleation of nanocellular foams.

solubility achieved during the saturation step. The IV is defined as the halo of diffusing gas.

The success of this theory relies on two main aspects. The first one assumes that a new nucleus can only be stably generated in the uninfluenced volume (UV) of the polymer (Fig. 8(b)), this being because inside the IV the gas molecules diffuse preferably into the already stable one. This leads to a smaller nucleation ratio, in agreement with experimental data. Additionally, the introduction of IV allows considering in the model that nucleation does not occur instantaneously, allowing the introduction of the influence

of parameters such as viscosity, diffusivity or pressure drop rate on the cellular structure.

Taking into account this theory, the differences observed between the materials produced using PMMA samples with different viscosities can be discussed.

Influence of viscosity on nucleation. The IV model assumes non-instantaneous nucleation, meaning that cells nucleated first grow to the detriment of the surrounding ones. Consequently, a greater IV will decrease the nucleation rate. This means that a slow growth rate of the initial nuclei is beneficial for the creation of new stable nuclei; this slow growth is promoted by high viscosity. A more viscous polymer provides more resistance to cell growth slowing down the increase of the IV and therefore leading to higher nucleation density. This contribution is given by the Schmidt number³⁵ that measures the relative effects of viscous diffusion over mass diffusion:

$$N_{Sc} = \frac{\mu}{\rho D} \tag{3}$$

where μ is the viscosity of the polymer/gas mixture, ρ is the density and D is the diffusion parameter.

Then, assuming the same amount of gas, HV can produce a greater number of nucleation points than MV and LV because the

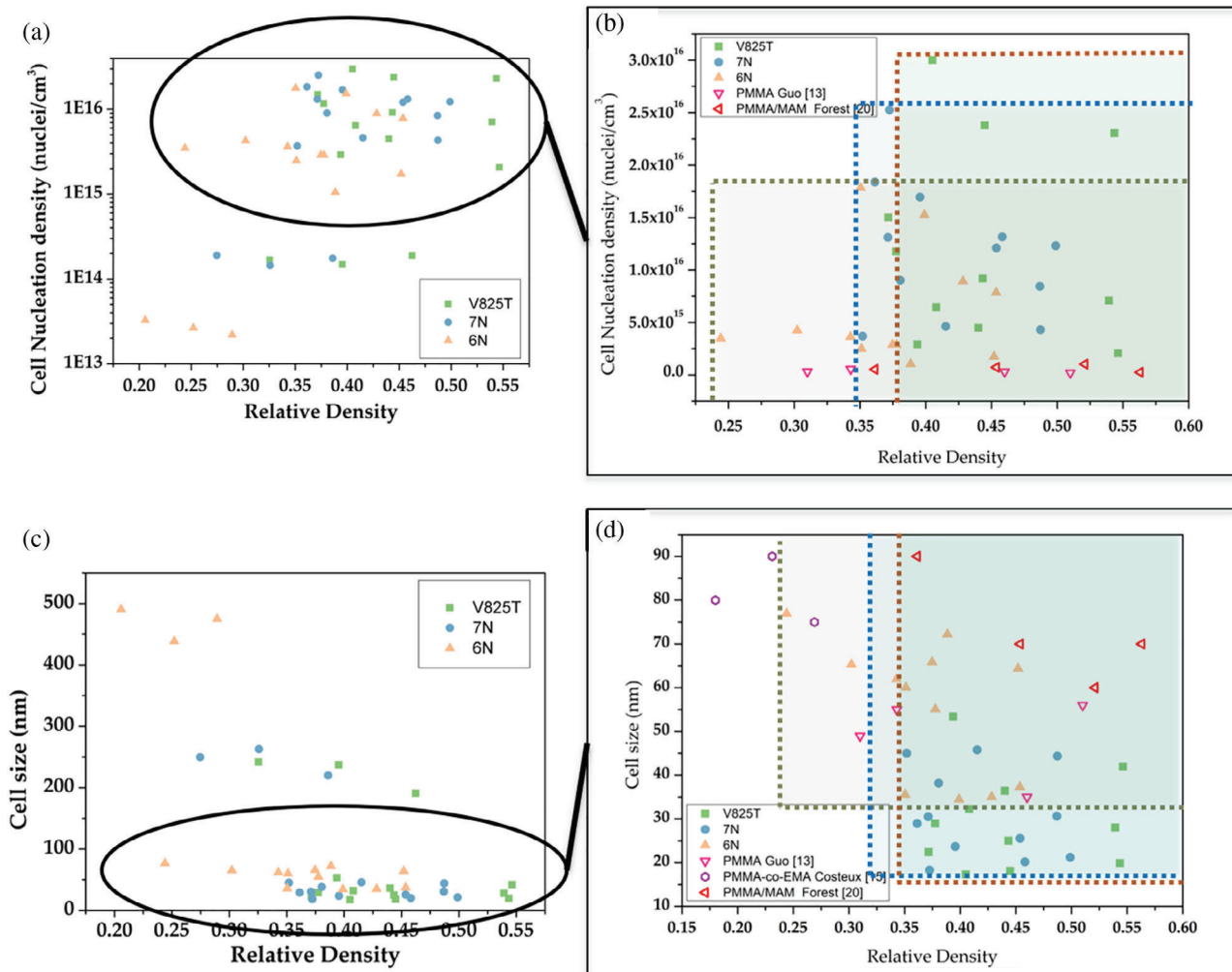


Figure 9. Maps of all the cellular materials produced.

IV is maintained smaller during the nucleation phase. This reasoning explains the results obtained at low saturation temperatures, where the solubility of the three materials is similar.

On the other hand, when saturating at room temperature, the solubility of LV is around 5% higher than that of HV and MV, which according to CNT will lead to higher N_0 . However, this higher solubility also results in a lower $T_{g,eff}$ and therefore a lower viscosity. According to the obtained results, this lower viscosity would lead to a large IV, which prevents the formation of a greater number of nucleation sites, resulting in a smaller cell nucleation density for the materials with lower viscosities.

Influence of viscosity on cell growth. One of the most common equations describing the growth rate of a single cell is^{34,36}

$$\frac{dR}{dt} = \frac{\Delta P \cdot R}{4\eta} - \frac{\gamma}{2\eta} \tag{4}$$

where γ is the interfacial tension between gas bubble and polymer, ΔP the pressure difference between the inner part of the samples and the environment and η the viscosity of the polymer/gas mixture.

Herein a decrease in the viscosity leads to an increase of the growth rate, which means that nuclei with the same size will grow

faster in LV. Explaining the results, Fig. 7(b) shows that LV presents larger cell sizes for any used condition.

On the other hand, the ability for cell growth and therefore the ability to reduce the relative density have been experimentally proved to be reduced as the amount of gas increases independent of the polymer used. This result can be again explained with the IV concept. Considering Eqn (4), an increase in ΔP will lead to a faster cell growth that will consume faster the IV that is providing gas to the cell. Moreover, the nucleation rate is proportional to the exponential of $1/\Delta P^2$ meaning that the rate of nucleation is higher than the growth rate.

In conclusion, gas is consumed in creating more cells that grow faster and less, due to the rapid decrease of IV. An interconnected cellular structure accompanies this fact. When the cells become open, the gas fast diffuses out of the cellular structure, and then further growth is prevented.

In conclusion, the ability of the material to expand is strongly determined by the viscosity of the polymer, possibly leading to smaller relative densities as the viscosity decreases. However, this expansion ability decreases with an increase of the solubility, it being more difficult to achieve lower densities when cell size is reduced.

Finally, the stabilization of the cellular structure should be done at a temperature lower than the effective glass transition of the

polymer to freeze the cellular structure. If the foaming temperature is too high or the foaming time too long, degeneration mechanisms appear during growth, and the structure collapses. For the materials under study, this happens when the foaming temperature is fixed at 100 °C for the materials with low and medium viscosity and at 110 °C for the material with higher viscosity.

Maps in Fig. 9 show the wide range of cellular materials produced in this work. Moreover, data from the literature of nanocellular PMMA with cell sizes below 100 nm are shown. The combination of using materials with different rheological properties and different saturation and foaming conditions allows the production of cellular materials with characteristics not reported before.

On the one hand, the most viscous material is capable of reaching the highest nucleation densities and the smallest cell sizes, but the minimum relative density achievable is around 0.37. On the other hand, LV covers regions of the materials maps (Fig. 9) only reported before by Costeux *et al.* using a P(MMA-co-EMA) copolymer.¹⁹

This study brings versatility to the production of nanocellular PMMA with a wide range of cell sizes, from 14 to 500 nm. The selection of the viscosity of the PMMA allows control of the final characteristics of the foams inside certain boundaries that have been established.

CONCLUSIONS

The influence of the viscosity of PMMA on the density and cellular structure of nanocellular polymers produced by gas dissolution foaming has been studied. It has been found that the viscosity affects the different steps, nucleation growth and stabilization, playing a key role in the density and the final cellular structure obtained.

It has been demonstrated that a lower viscosity leads to a smaller number of nucleation points even for larger solubilities. This effect can be attributed to the ability of the viscosity to control the IV; a higher viscosity slows down the evolution of IV, leading to the creation of a greater number of cells. Moreover, the viscosity plays an essential role in the growth process, it being beneficial to have low viscosity for further expansion, these effects being more pronounced at low solubilities.

Solubility is influenced by the processing parameters, also playing an essential role in the cellular materials obtained. A high solubility makes smaller the differences between polymers increasing the nucleation rate, reducing the growth of the cells and creating interconnected cellular structures.

On the other hand, with the same solubility, a change in the foaming conditions allows one to obtain a wide range of cellular structures and densities. An increase in the foaming temperature leads to cellular materials with almost the same cell size but a higher cell nucleation density resulting in a lower relative density.

In this work, by combining the use of raw materials with different viscosities and different processing parameters, nanocellular materials with cell sizes in the range 14 to 500 nm and cell nucleation densities from 10^{13} to 10^{16} nuclei cm^{-3} have been produced. Among all these cellular materials, we can highlight the production of a nanocellular polymer with a cell size of 75 nm and a cell nucleation density of 10^{15} nuclei cm^{-3} combined with a relative density of 0.24 using a low-viscosity PMMA. On the other hand, using a high-viscosity material is possible to produce nanocellular polymers with a cell size of 14 nm, 3.5×10^{16} nuclei cm^{-3} and a relative density of 0.4.

It has been shown that appropriate control of the rheological properties of PMMA is essential for fine-tuning the cellular structure of nanocellular polymers.

ACKNOWLEDGEMENTS

Financial assistance from MINECO, FEDER, UE (MAT2015-69234-R), the Junta of Castile and Leon (VA275P18) and Spanish Ministry of Science, Innovation and Universities (RTI2018-098749-B-I00) is gratefully acknowledged. Financial assistance from EREN (Ente Regional de la Energía de Castilla y León, EREN_2019_L4_UVA) is gratefully acknowledged. Financial support from FPU grant FPU14/02050 (VB) from the Spanish Ministry of Education and Junta of Castile and Leon grant (JM-L) are gratefully acknowledged. Financial support from MINECO PTQ-16-08248 (EL-G) is gratefully acknowledged.

SUPPORTING INFORMATION

Supporting information may be found in the online version of this article.

REFERENCES

- 1 Kumar V and Suh NP, *Polym Eng Sci* **30**:1323–1329 (1990).
- 2 Shimbo M, Higashitani I and Miyano Y, *J Cell Plast* **43**:157–167 (2007).
- 3 Kumar V, Weller JE, Ma M, Montecillo R and Kwapisz RR, *Cell Polym* **17**:350–361 (1998).
- 4 Notario B, Pinto J, Solorzano E, De Saja JA, Dumon M and Rodriguez-Perez MA, *Polymer* **56**:57–67 (2015).
- 5 Notario B, Pinto J and MA R-P, *Polymer* **63**:116–126 (2015).
- 6 Martín-de León J, Bernardo V and Rodriguez-Perez MA, *Macromol Mater Eng* **302**:1700343 (2017).
- 7 Martín-de León J, Bernardo V and Rodríguez-Pérez M, *Materials* **12**:797 (2019).
- 8 Martín-de León J, Pura JL, Bernardo V and Rodríguez-Pérez MÁ, *Polymer* **170**:16–23 (2019).
- 9 Liao R, Yu W and Zhou C, *Polymer* **51**:568–580 (2010).
- 10 Leung SN, Wong A, Guo Q, Park CB and Zong JH, *Chem Eng Sci* **64**:4899–4907 (2009).
- 11 Ludwiczak J, Frackowiak S and Łuzny R, *Cell Polym* **37**:69–79 (2018).
- 12 Costeux S, Bunker SP and Jeon HK, *J Mater Res* **28**:2351–2365 (2013).
- 13 Forest C, Chaumont P, Cassagnau P, Swoboda B and Sonntag P, *Polymer* **77**:1–9 (2015).
- 14 Guo H and Kumar V, *Polymer* **56**:46–56 (2015).
- 15 Bernardo V, Martín-De León J and Rodríguez-Pérez MA, *Mater Lett* **178**:155–158 (2016).
- 16 Guo H and Kumar V, *Polymer* **57**:157–163 (2015).
- 17 Pinto J, Dumon M, Pedros M, Reglero J and Rodriguez-Perez MA, *Chem Eng J* **243**:428–435 (2014).
- 18 Bernardo V, Martín-de León J, Laguna-Gutierrez E, Catelani T, Pinto J, Athanassiou A *et al.*, *Polymer* **153**:262–270 (2018).
- 19 Costeux S, Jeon MH, Bunker TS, Khan I, Nanocellular, Foam 2012 Conference, pp. 1–6 (2012).
- 20 Costeux S and Zhu L, *Polymer* **54**:2785–2795 (2013).
- 21 Bernardo V, Martín-de León J, Laguna-Gutiérrez E and Rodríguez-Pérez MÁ, *Eur Polym J* **96**:10–26 (2017).
- 22 Martín-de León J, Bernardo V and Rodríguez-Pérez M, *Polymers* **8**:265 (2016).
- 23 Pinto J, Reglero-Ruiz JA, Dumon M and Rodriguez-Perez MA, *J Supercrit Fluids* **94**:198–205 (2014).
- 24 Guo H and Kumar V, Some thermodynamic and kinetic low-temperature properties of the PC-CO₂ system and morphological characteristics of solid-state PC nanofoams produced with liquid CO₂. *Polymer* **56**:46–56 (2015).
- 25 Crank J, *The Mathematics of Diffusion*. Oxford University Press, Oxford (1975).
- 26 Pinto J, Solorzano E, Rodriguez-Perez M a and de Saja J a, *J Cell Plast* **49**:555–575 (2013).

- 27 Kumar V and Suh NP, *Polym Eng Sci* **30**:1323–1329 (1990).
- 28 Laguna-Gutierrez E, Van Hooghten R, Moldenaers P and Angel Rodriguez-Perez M, *J Appl Polym Sci* **132**:1–12 (2015).
- 29 Handa YP, Zhan Z and Wong B, *Cell Polym* **20**:1–16 (2001).
- 30 Martín-de León J, Bernardo V and Rodríguez-Pérez MÁ, *Macromol Mater Eng* **3**:1700343 (2017).
- 31 Rindfleisch F, DiNoia TP and McHugh MA, *J Phys Chem* **100**:15581–15587 (1996).
- 32 Kaufman HS, Falcetta JJ and Falcetta JJ, *Introduction to Polymer Science and Technology: An SPE Textbook*. Wiley, New York (1977).
- 33 Tang M, Du T-B and Chen Y-P, *J Supercrit Fluids* **28**:207–218 (2004).
- 34 Costeux S, Khan I, Bunker SP and Jeon HK, *J Cell Plast* **51**:197–221 (2014).
- 35 Bergman TL and Incropera FP, *Fundamentals of Heat and Mass Transfer*. Wiley, New York (2011).
- 36 Khan I, Adrian D and Costeux S, *Chem Eng Sci* **138**:634–645 (2015).